Acta Acustica 2022, **6**, 41

https://doi.org/10.1051/aacus/2022036

Available online at:
https://acta-acustica.edpsciences.org

TECHNICAL & APPLIED ARTICLE OPEN ACCESS

Formation process of thermal damage in a target area of high intensity focused ultrasound and effectiveness analysis of B-ultrasound real-time monitoring

Peng Zhao[1,2], Yuebing Wang[1,2], Yanqi Wu[2,*], Xiaoye Hu[3], Hong Shen[3], Shiqi Tong[2], and Jie Tao[2]

[1] College of Optoelectronic Engineering, Changchun University of Science and Technology, Changchun 130013, China
[2] College of Metrology and Measurement Engineering, China Jiliang University, Hangzhou 310018, Zhejiang, China
[3] Department of Medical Oncology, Second Affiliated Hospital, Zhejiang University School of Medicine, Hangzhou 310009, Zhejiang, China

Received 2 June 2022, Accepted 24 August 2022

Abstract – High intensity of focused ultrasound (HIFU) is an effective tumor therapy, taking advantage of the thermal effect and cavitation effect to generate thermal damage to the target tissue. However, inaccurate ultrasonic dose control may result in ineffective or excessive treatment. Thus, real-time monitoring of the thermal damage formation process is critical. To evaluate the effectiveness of real-time monitoring of B-ultrasound, ex-vivo bovine livers were irradiated by 1.155 MHz focused ultrasound with emission time $T1$ of 200 ms and interval time $T2$ of 200 ms. For orthogonal experiments, ultrasound was irradiated at sound power of 100 W, 125 W, and 150 W for 10 s, 20 s, and 40 s, respectively. B-ultrasound image sequences are collected using a 7.5 MHz linear array and compared with backscattered echo signals and thermal damage slices, respectively, to build relationships between B-mode ultrasound monitoring and thermal effect or cavitation effect. The experimental results demonstrated that the tissue ablation process caused by thermal effect cannot be effectively monitored using B-ultrasound, but the process caused by the cavitation effect can. The analysis revealed a strong temporal correlation between the appearance of bright spots in B-ultrasound images and the sudden increase of the scattered echo power spectrum, which were caused by a large number of microbubbles from cavitation. The damaged cavity structure of the slices and the development trend of microbubbles showed a strong spatial correlation. Furthermore, the sudden increase in the scattered echo signal shows the potential of early warning of cavitation, as it is 1.2–2.0 s ahead of the bright spot in the B-ultrasound image, laying the experimental basis for improving the effectiveness of B-ultrasound monitoring in clinical HIFU surgery.

Keywords: High intensity focused ultrasound, Thermal damage, Cavitation, B-ultrasound imaging, Real-time monitoring

1 Introduction

As non-invasive, non-ionizing radiation, non-invasive treatment, high-intensity focused ultrasound (HIFU) has been widely used to treat solid tumors such as uterine fibroids [1], liver cancer [2], bone tumors [3], breast cancer [4] and pancreatic cancer [5] and is an effective complement to traditional surgery. The primary goal of HIFU treatment is to cause instantaneous coagulation and necrosis in the target tissue, which is then absorbed or scarred. HIFU treatment works via a variety of mechanisms, including thermal effect [6], cavitation effect [7, 8], mechanical effect [9], biological effect [10] and so on, with thermal effect and cavitation effect playing a significant role. Due to the complexity and uncontrollability of the mechanisms, it is critical for the demand for safe treatment to have an effective and real-time process monitoring of the thermal damage.

Several methods for monitoring in surgery are currently available, including computed tomography (CT) [11], magnetic resonance imaging (MRI) [12], and B-mode ultrasonography [13]. CT and MRI have a high degree of imaging accuracy but a limited ability to perform in real-time. Meanwhile, the operation is inconvenient, which means it is not conducive to real-time monitoring during surgery but rather to preoperative diagnosis and postoperative evaluation. Ultrasonic imaging collects and analyzes scattered echo waves generated when ultrasound penetrates tissue to characterize the difference in acoustic impedance and generate a gray-scale image. Its advantages include

*Corresponding author: wuyanqi@cjlu.edu.cn

real-time monitoring, complete non-destructive examination, the absence of ionizing radiation, low cost, and ease of integration with treatment equipment. It is widely used in real-time monitoring of HIFU treatment.

Zhao et al. [14, 15] reported the treatment of low-power accumulation. Clinical data demonstrated clear survival benefits and a favorable safety profile in patients with malignant tumors. Among them, the high duty cycle $T1/T2$ 990 ms/10 ms treatment scheme enables clinicians to monitor tumor tissue changes using B-ultrasound only during the treatment's idle time, as the sound wave irradiated by HIFU will appear as strong background noise on the B-ultrasound image, resulting in low imaging accuracy and inability to meet the requirements of intraoperative real-time monitoring. On the other hand, therapeutic ultrasound does not affect B-ultrasound imaging in treatment schemes with a relatively low duty cycle $T1/T2$ 200 ms/200 ms. It is expected to realize real-time monitoring of the treatment process.

To gain a thorough understanding of the development characteristics of target thermal damage during low-power cumulative treatment and to assess the real-time monitoring effect of B-ultrasound imaging, degassed ex-vivo bovine liver was used as an experimental sample and irradiated with a range of HIFU energies, sound powers, and irradiation durations. A 128-element 7.5 MHz linear array and a receiving transducer were used to collect B-ultrasound images and scattered echo signals, respectively. By analyzing the B-ultrasound images, reflected acoustic spectrum, and thermal damage slice, a correlation between the strong echo of B-ultrasound and the formation process of thermal damage was established. This provides an experimental basis for the effectiveness of B-ultrasound monitoring in clinical HIFU surgery.

2 Materials and methods

The experimental setup is shown in Figure 1. A confocal transducer composed of a transceiver developed by ourself is attached to the sidewall of a plexiglass transparent water tank, whose size is 220 mm × 130 mm × 130 mm. The tank was filled with degassed water within less than 0.3 mg/L gas. The degassed ex-vivo bovine liver was cut into 50 mm × 50 mm × 50 mm segments and placed in a square polycarbonate box with holes on six sides and fixed at the focus of the focusing transducer. A 7.5 MHz B-ultrasound probe (L7.5AS, S-Sharp, Taiwan, China) is placed directly above the bovine liver, parallel to the direction of the acoustic axis, and its position and posture can be adjusted using a 3-D x–y–z positioner.

2.1 HIFU transducer and driving system

The aperture of the spherical shell transducer used for transmitting sound waves is 95 mm, with a 22 mm hole in the middle. The resonant frequency is 1.155 MHz, the geometric focal length is 150 mm, the −6dB focus size is 30 mm × 3 mm (axial × radial). Two channels arbitrary

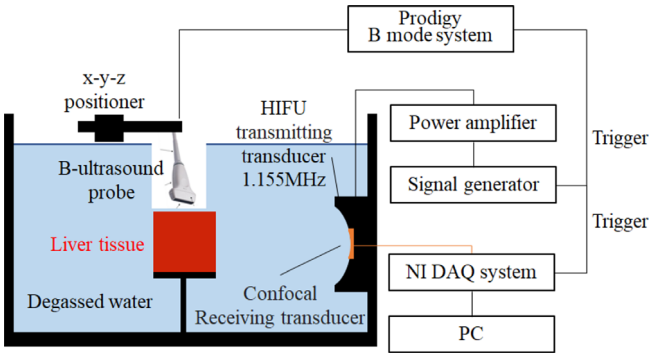

Figure 1. Experimental setup.

signal generator (DG5072, RIGOL, China) is used to generate excitation signal. CH1 generates a gate signal with a period of 400 ms, CH2 generates a continuous sine wave of 1.155 MHz, which is modulated by the gate signal and output to the power amplifier (AR800W, AR, USA), driving the transmitting transducer to irradiate ultrasonic wave. The working sequence is shown in Figure 2.

The spherical shell transducer emits a 200 ms high-intensity sound wave followed by a 30 μs detection sound wave after a 300 μs delay in a 400 ms periodic sequence. For ultrasonic echo signal acquisition and B-ultrasound imaging, the echo signal acquisition system and the B-ultrasound acquisition system are triggered simultaneously. Before the experiment began, the sound power was determined [16], as shown in Table 1.

2.2 Echo signal acquisition system

A confocal receiving transducer with an aperture of 20 mm and a geometric focal length of 150 mm is installed in the middle of the transmitting transducer. The transducer receives the echo signal, and the NI-DAQ system (PXI-5105, National Instruments, USA) samples the voltage signal at 60 MHz/8 bits. The time-domain echo signal is collected, and the variation of scattering echo with HIFU irradiation is analyzed offline using the power spectrum by LabVIEW (LabVIEW2019, National Instruments, USA).

2.3 B-ultrasound imaging method

During the HIFU irradiation process, a 128-element linear array B-ultrasound probe with a center frequency of 7.5 MHz is placed above the bovine liver and fine-tuned using a 3D x–y–z positioner to ensure that the B-ultrasound probe is parallel to the sound axis direction. A B-ultrasound imaging system (Prodigy256, S-Sharp, Taiwan, China) set to pulse sequence (PS), and external trigger mode collects, analyzes, displays, and stores the data. It takes approximately 200 ms to image a frame of B-ultrasound sequence that is triggered by the rising edge of the detecting sound wave's gate signal, as shown in Figure 2. Each subarray is driven by the B-ultrasound imaging system, which transmits a phase-controlled delay signal to focus the ultrasonic

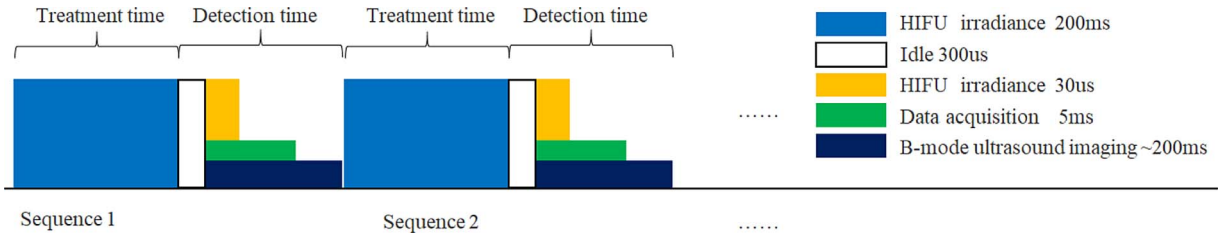

Figure 2. System working sequence.

Table 1. Sound power setting conditions.

No.	Sine wave peak (mVpp)	Amplifier gain (%)	Isal (kW/cm^2)	Acoustic power (W)
1	370	58	1.42	100
2	390	59	1.77	125
3	510	56	2.12	150

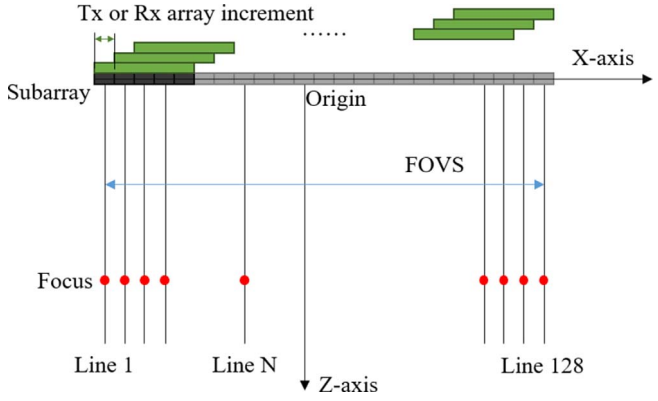

Figure 3. Principle of B-ultrasound imaging.

wave at a predetermined depth and receives a beamformed signal to determine the gray value of a line. As illustrated in Figure 3, different subarrays are selected in this manner to obtain the entire normalized gray image.

2.4 Experimental arrangement

Fresh bovine liver slaughtered within 6 h was bought from the slaughterhouse and cut into 50 mm × 50 mm × 50 mm regular shape. Homogeneous samples without thick blood vessels or fascia are selected and equally divided into three groups. Repetitive orthogonal experiments are conducted with samples being irradiated by such ultrasonic power as 100 W, 125 W, and 150 W for 10 s, 20 s, and 40 s, respectively. The ultrasonic dose is defined as power × exposure time in this paper. Low power × short exposure time is defined as low dose. In contrast, high power × long exposure time is defined as high dose. The other situation between the two is defined as medium dose. B-ultrasonic image sequence, thermal damage slice image, and the original waveform of scattering echo signal are obtained simultaneously and analyzed offline under each condition of ultrasonic dose.

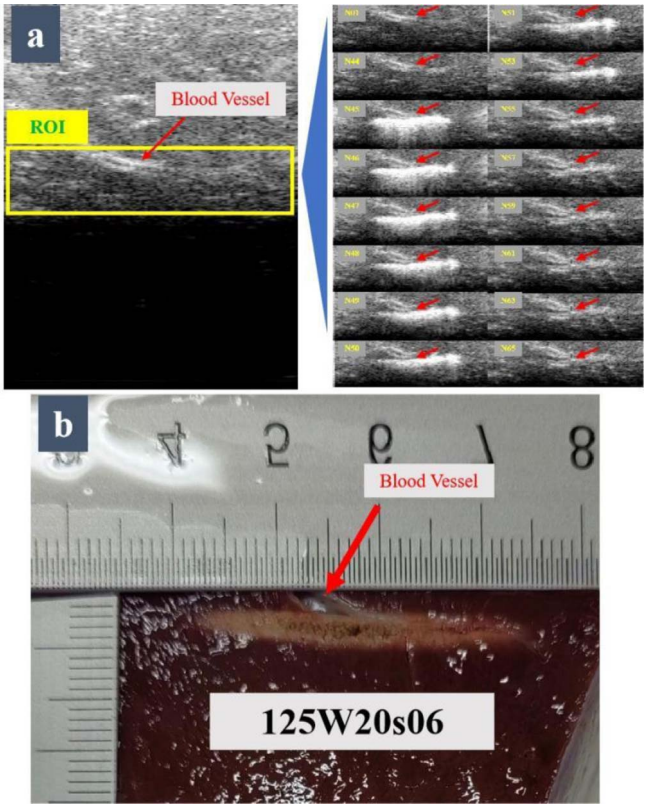

Figure 4. B-ultrasound image and damage slice in 125W20s case (a) B-ultrasound image, with red arrows pointing to such special tissue structure as blood vessels as spatial reference. (b) Damage slice.

3 Results

3.1 Result analysis method

The B-ultrasound system triggered by the rising edge presents images in a 400 ms cycle. The resolution of each frame image is 512 × 512. Region of interest (ROI) sequences covering the physical focal region of HIFU of 120 × 400 pixels, as shown in Figure 4a, are selected to observe the changes caused by HIFU irradiation over time.

As shown in Figure 4b, ex-vivo bovine liver samples are sliced, and the shape, size, and degree of thermal ablation damage are measured compared to the B-ultrasound image. The obvious temporal and spatial characteristics are observed using the specific tissue structure in the bovine liver, blood vessels for example, as a reference mark position

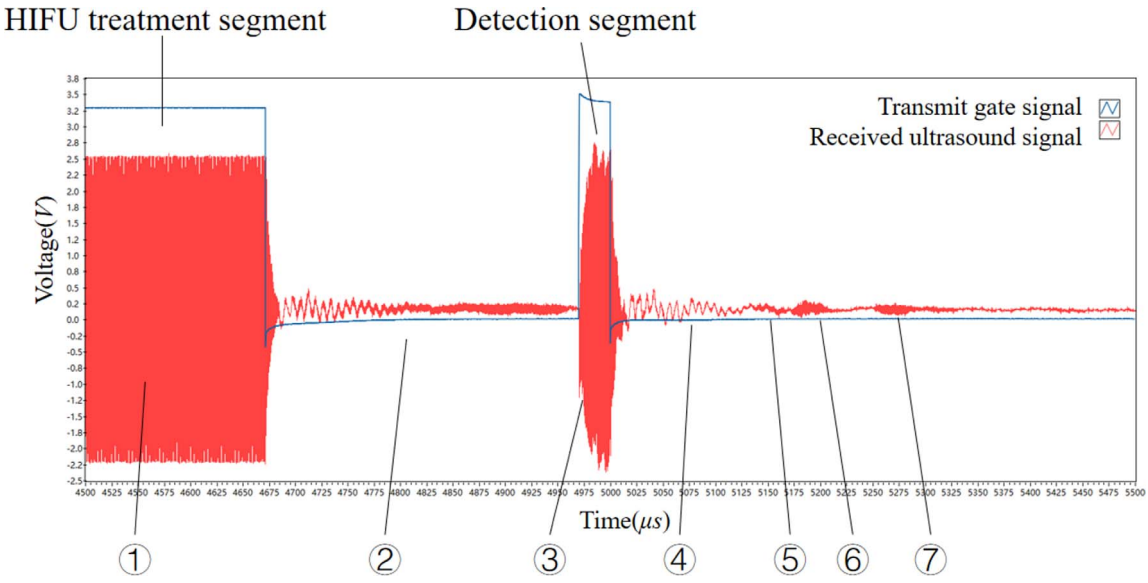

Figure 5. Reflected and scattered echo waveform (frame No. 25 in 125W20s case).

and analyzing the relationship between B-ultrasound images and the final morphology and size of bovine liver thermal damage.

The reflected and scattered echo waveforms collected by the NI-DAQ system are shown in Figure 5. The signal components of sections ①–④ of the figure are so complex, including the direct wave irradiated by HIFU, the reflected echo of the multi-layer interface of bovine liver tissue, the scattered echo generated within the tissue, and the vibration signal caused by the radial vibration mode of the transmitting transducer, determining that they cannot be useful for power spectrum analysis. However, the signals in the figure representing segments ⑤–⑦ are pure echo ultrasonic signals. Among them, segment ⑤ represents the reflected wave on the front surface of the bovine liver. Segment ⑥ is the scatter echo caused by the internal structure change of the bovine liver, and segment ⑦ is the reflected wave on the rear surface of the water tank. Thus, the change of scatter echo ⑥ is the focus of our attention in this paper. The power spectrum of the waveform is calculated, and the variation law of the energy of the fundamental frequency component is analyzed.

3.2 Low ultrasonic dose irradiation

On B-ultrasound images, 100 W cases with exposure times of 20 s, 30 s, and several 40 s, and 125 W cases with exposure times of 10 s exhibit no significant changes. However, as illustrated in Figure 6, the slices have obvious thermal damage in the shape of a slender jujube nucleus. As shown in Table 2, the ultrasound dose and ablation size were statistically analyzed. As a result, it can be concluded that the ablation first develops axially to the transducer side along the acoustic axis and then gradually expands radially.

The changing curves of the power spectrum of the scattered echo's 1.155 MHz fundamental frequency component are shown in Figure 7. The time-varying curve demonstrates that when the dose is low, the energy of the echo signal fluctuates gently, exhibiting a trend of periodic oscillations weakening first and then strengthening overall, but never a sudden change.

3.3 Medium and high ultrasonic dose irradiation

With low power and a long exposure time in the 100W40s case, as shown in Figure 8b, a large area of bright spots appears suddenly in frame 63 of the B-ultrasound image. It then moves relatively slowly in the direction of the transducer, reaching its maximum size at frame 110. At this point, HIFU ceases irradiation, and the bright spots gradually fade away. The ablation slice is shaped like a "tadpole", and cavities are located in the spatial distribution's center and rear. With an increase in ultrasonic dose, as shown in Figure 8d, slender bright spots appeared suddenly in the B-ultrasound image at frame 35, and the bright spots rapidly moved towards the transducer in the 125W20s case. At frame 52, the HIFU irradiation was stopped, and the bright spots gradually disappeared. The ablation shape is slender, and cavities are distributed evenly throughout the spatial distribution. Similarly, in the case of the 150W20s, as shown in Figure 8f, small bright spots appear on B-ultrasound in frame 14 and migrate towards the transducer while maintaining a small area. At frame 50, the HIFU irradiation is stopped, and the bright spots gradually fade away. Thermal damage is shaped like a "tadpole", with cavities throughout the spatial distribution.

The changing curves of the power spectrum of the scattered echo's 1.155 MHz fundamental frequency component are shown in Figure 9. It is discovered that when a medium or high ultrasonic dose is irradiated, the energy of the echo signal fluctuates gently in the preceding period, similar to the situation when a low ultrasonic dose is irradiated. However, at frame 60 of 100W40s, a sudden increase in energy occurs. Thus, as with frame 31 in the 125W20s case and

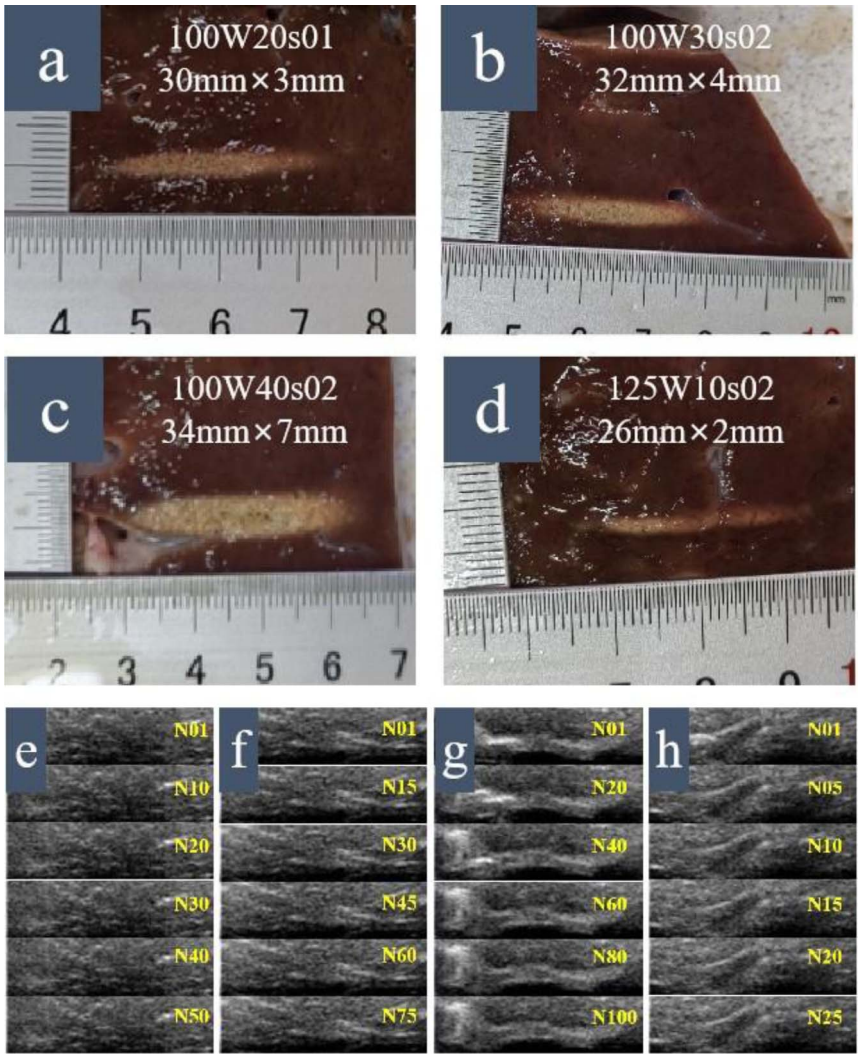

Figure 6. Thermal damage slices and B-ultrasound images (a) and (e) 100W20s, (b) and (f) 100W30s, (c) and (g) 100W40s, (d) and (h) 125W10s.

Table 2. Low dose ablation size statistics.

Ultrasonic dose	Ablation size	Aspect ratio
100 W × 20 s	30 mm × 3 mm	10.00
100 W × 30 s	32 mm × 4 mm	8.00
100 W × 40 s	32 mm × 7 mm	4.57
125 W × 10 s	26 mm × 2 mm	13.00

frame 9 in the 150W20s case, respectively, there is a period of strong discrete fluctuation followed by a period of continuous fluctuation until the end of the exposure.

The frame number N_{echo} at which the scattered echo suddenly increases, the frame number N_{B} of the bright spots occurrence on the B-ultrasound image, the final ablation size and the location of the damaged cavity (F-Front, M-Middle, B-Back) are analyzed statistically as Table 3. According to the analysis in low ultrasonic dose irradiation, there will be no bright spots on B-ultrasound in low ultrasonic dose cases. However, it is uncertain in low power × long expose time cases, as shown in Figure 8a, with the ablation shape of which is generally "tadpole". Additionally, in cases of medium to high ultrasonic dose radiation, there will be obvious bright spots on B-ultrasound images.

4 Discussion

The thermal effect is a significant factor in low-dose HIFU radiation therapy. Heat is converted and deposited because of the attenuation of ex-vivo tissue on sound waves in the tissue, resulting in a temperature rise above 65 °C and the formation of permanent protein coagulation necrosis. As shown in Table 1, thermal damage develops rapidly in the axial direction early in the treatment and gradually in the radial direction later in the treatment. This treatment scheme has a lower efficiency but produces more regular "jujube nucleus" shaped thermal ablation, as illustrated in Figure 6. B-ultrasound is ineffective at monitoring the ablative area and its formation during treatment.

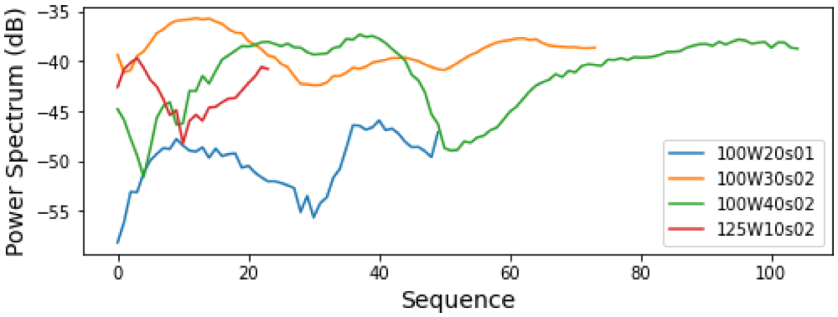

Figure 7. Power spectrum analysis of scattered echo signal with low ultrasonic dose irradiation.

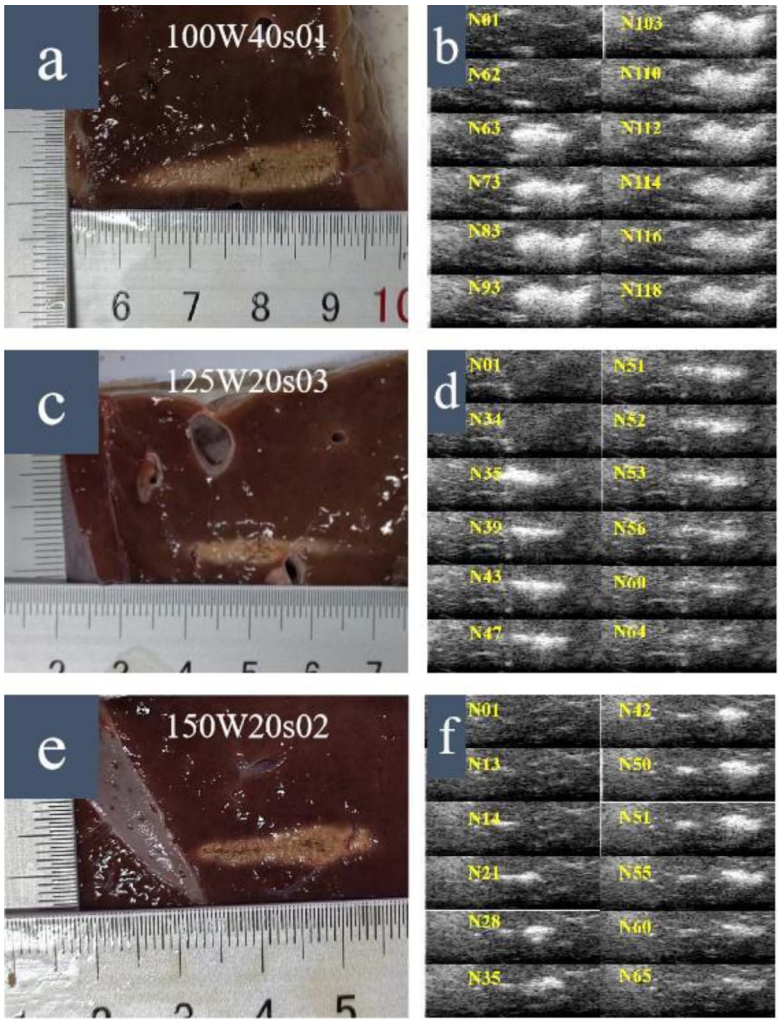

Figure 8. Thermal damage slices and B-ultrasound images (a) and (b) 100W40s, (c) and (d) 125W20s, (e) and (f) 150W20s.

This requires clinicians to use MRI or contrast-enhanced intraoperative ultrasound to precisely determine the ablated area's size and precisely control the ultrasonic dose. However, the treatment will become uncontrollable if the exposure time is extended indefinitely in the low ultrasonic power case. When bright spots appear on B-ultrasound images, the resulting damage takes on the shape of a "tadpole" as illustrated in Figure 8a.

The thermal effect is dominant at the early stages of medium-dose HIFU irradiation. Cavitation will occur later, significantly increasing thermal efficiency, as illustrated in Figure 8a and 8b. While B-ultrasound can monitor the cavitation effect, it cannot monitor the thermal effect. Due to the formation of thermal damage during the early stages of treatment, the reflection of a transmitted therapeutic sound wave is enhanced, causing the thermal

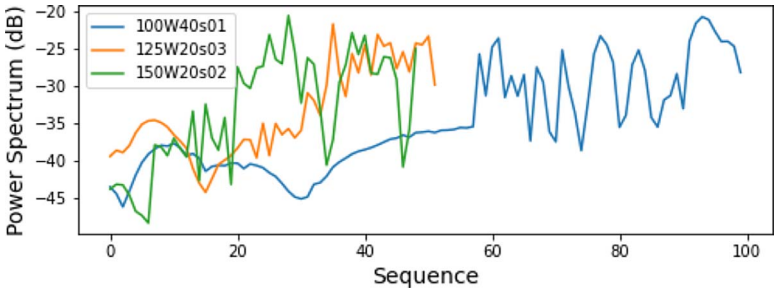

Figure 9. Power spectrum analysis of scattered echo signal with medium and high ultrasonic dose irradiation.

Table 3. Medium and high dose ablation statistics.

No.	Ultrasonic dose	N_{echo}	N_B	Ablation size	Cavity position
1	100 W × 40 s	60	63	30 mm × 7 mm	M
2	100 W × 40 s	84	90	23 mm × 5 mm	B
3	125 W × 20 s	31	35	26 mm × 4 mm	M&B
4	125 W × 20 s	31	32	23 mm × 5 mm	F&B
5	125 W × 20 s	68	70	35 mm × 4 mm	B
6	150 W × 10 s	7	11	12 mm × 3 mm	M
7	150 W × 20 s	9	12	21 mm × 4.5 mm	F&M&B
8	150 W × 20 s	11	12	20 mm × 4 mm	F&M

damage to moving toward the transducer. The temperature rise and the continuous action of high acoustic negative pressure precipitate microbubbles in the ex-vivo tissue, and cavitation occurs when the condition exceeds the cavitation threshold, significantly exacerbating the thermal effect. Simultaneously, the presence of bubble clusters alters the acoustic impedance characteristics of the local tissue, resulting in visible bright spots on B-ultrasound images. For high-dose HIFU irradiation, increasing the ultrasonic power advances both the temporal and spatial location of cavitation occurrence, as illustrated in Figure 8e–8f. Under this treatment scheme, doctors can roughly estimate the shape and size of thermal damage based on bright spots on B-ultrasound images but should keep in mind that the B-ultrasound image is a normalized gray image and thus cannot quantify the size of thermal damage precisely.

When cavitation occurs suddenly during HIFU irradiation, the scattered echo also increases immediately with a large time-varying discreteness, which can be used as important evidence of the cavitation effect. Additionally, this sudden strong oscillation occurs approximately 3–5 frames before the appearance of bright spots on B-ultrasound images, corresponding to an exposure time of 1.2–2.0 s, requiring clinicians to address the cavitation situation as soon as possible when they see bright spots on B-ultrasound images, to avoid uncontrollable terrible consequences.

After HIFU irradiation is stopped, the bright spots on the B-ultrasound images gradually darken until they vanish, as a large number of microbubbles precipitated as a result of cavitation quickly burst and vanish, demonstrating once again that the bright spots observed on the B-ultrasound images are microbubbles generated by cavitation, not thermal damage.

5 Conclusion

B-ultrasound is a critical tool for monitoring the HIFU treatment process in real-time. The following are the major conclusions drawn from this paper's research:

First, because thermal damage is always directed toward the transducer during HIFU irradiation, clinicians should locate the initial treatment point at the back of the tumor with a certain distance from the transducer rather than in the center. Otherwise, it will lead to incomplete treatment at the bottom of the tumor. In this way, the bottom of the tumor can be ablated by thermal diffusion.

Second, B-ultrasound is ineffective at monitoring thermal ablation because the bright spots visible in B-ultrasound represent the generation of cavitation, not the thermal effect. This means that clinicians should be assisted with intraoperative B-ultrasound angiography or MRI if the size of the total thermal damaged area needs to be precisely determined to avoid terrible accidents such as thermal scald or perforation caused by overtreatment.

Third, thermal damage is primarily caused by thermal effects in low sound power situations and cavitation effects in high sound power situations. In general, for the same ultrasonic dose, the thermal efficiency by low-power × long-time treatment mode is relatively lower, but the controllability is higher, giving physicians a longer response time. On the contrary, the high-power × short-time treatment mode has a higher thermal efficiency but a lower controllability, giving clinicians less response time in the

event of an emergency. Therefore, clinicians should select the most appropriate treatment mode for individual patients during clinical treatment.

Conflict of interest

The authors declare no conflict of interest.

Acknowledgments

This work was supported by National Key R&D Program of China (Grants 2018YFC0114902).

References

1. E. Maloney, J.H. Hwang: Emerging HIFU applications in cancer therapy. International Journal of Hyperthermia 31, 3 (2015) 302–309.
2. J.F. Aubry, K.B. Pauly, C. Moonen, G. Haar, M. Ries, R. Salomir, S. Sokka, K.M. Sekins, Y. Shapira, Y. Fangwei, H. Huff-Simonin, M. Eames, A. Hananel, N. Kassell, A. Napoli, J.H. Hwang, W. Feng, Z. Lian, A. Melzer, Y.-S. Kim, W.M. Gedroyc: The road to clinical use of high-intensity focused ultrasound for liver cancer: technical and clinical consensus. Journal of Therapeutic Ultras 1, 1 (2013) 1–7.
3. C. Li, W. Zhang, W. Fan, J. Huang, F. Zhang, P. Wu: Noninvasive treatment of malignant bone tumors using high-intensity focused ultrasound. Cancer 116, 16 (2010) 3934–3942.
4. F. Wu, Z.B. Wang, Y.D. Cao, W.Z. Chen, J. Bai, J.Z. Zou, H. Zhu: A randomised clinical trial of high-intensity focused ultrasound ablation for the treatment of patients with localised breast cancer. British Journal of Cancer 89, 12 (2003) 2227–2233.
5. A. Sofuni, Y. Asai, T. Tsuchiya, K. Ishii, R. Tanaka, R. Tonozuka, M. Honjo, S. Mukai, K. Nagai, K. Yamamoto, Y. Matsunami, T. Kurosawa, H. Kojima, T. Homma, H. Minami, R. Nakatsubo, N. Hirakawa, H. Miyazawa, Y. Nagakawa, A. Tsuchida, T. Itoi: Novel therapeutic method for unresectable pancreatic cancer-the impact of the long-term research in therapeutic effect of high-intensity focused ultrasound (HIFU) therapy. Current Oncology 28, 6 (2021) 4845–4861.
6. G.T. Haar: HIFU tissue ablation: concept and devices. Advances in Experimental Medicine and Biology 880 (2016) 3–20.
7. C.C. Coussios, C.H. Farny, G. Ter Haar, R.A. Roy: Role of acoustic cavitation in the delivery and monitoring of cancer treatment by high-intensity focused ultrasound (HIFU). International Journal of Hyperthermia 23, 2 (2007) 105–120.
8. V. Gryzunov, A. Zaycev, Y. Kim, D. Tkhai: Effects of collapsing cavitation on HIFU-exposed biological objects. East European Science Journal 3, 10 (74) (2021) 22–25.
9. H. Han, H. Lee, K. Kim, H. Kim: Effect of high intensity focused ultrasound (HIFU) in conjunction with a nanomedicines-microbubble complex for enhanced drug delivery. Journal of Controlled Release 266 (2017) 75–86.
10. F. Li, Z. Wang, Y. Du, P. Ma, J. Bai, F. Wu, R. Feng: Study on therapeutic dosimetry of HIFU ablation tissue. Journal of Biomedical Engineering 23, 4 (2006) 839–843.
11. A. Orlacchio, G. Bazzocchi, D. Pastorelli, F. Bolacchi, M. Angelico, C. Almerighi, S. Masala, G. Simonetti: Percutaneous cryoablation of small hepatocellular carcinoma with US guidance and CT monitoring: initial experience. Cardiovascular and Interventional Radiology 31, 3 (2008) 587–594.
12. B.D. de Senneville, C. Moonen, M. Ries: MRI-guided HIFU methods for the ablation of liver and renal cancers. Advances in Experimental Medicine and Biology 880 (2016) 43–63.
13. M.S.R. Gudur, R.E. Kumon, Y. Zhou, C.X. Deng: High-frequency rapid B-mode ultrasound imaging for real-time monitoring of lesion formation and gas body activity during high-intensity focused ultrasound ablation. IEEE Transactions on Ultrasonics, Ferroelectrics, and Frequency Control 59, 8 (2012) 1687–1699.
14. J. Zhao, F. Zhao, Y. Shi, Y. Deng, X. Hu, H. Shen: The efficacy of a new high intensity focused ultrasound therapy for locally advanced pancreatic cancer. Journal of Cancer Research and Clinical Oncology 143, 10 (2017) 2105–2111.
15. J. Zhao, H. Shen, X. Hu, Y. Wang, Y. Yuan: The efficacy of a new high-intensity focused ultrasound therapy for metastatic pancreatic cancer. International Journal of Hyperthermia 38, 1 (2021) 288–295.
16. W. Shou, X. Huang, S. Duan, R. Xia, Z. Shi, X. Geng, F. Li: Acoustic power measurement of high intensity focused ultrasound in medicine based on radiation force. Ultrasonics 44 (2006) e17–e20.

Cite this article as: Zhao P. Wang Y. Wu Y. Hu X. Shen H, et al. 2022. Formation process of thermal damage in a target area of high intensity focused ultrasound and effectiveness analysis of B-ultrasound real-time monitoring. Acta Acustica, **6**, 41.